Supporting Information

Burkhardt et al. 10.1073/pnas.1106189108

SI Experimental Procedures

Structure Determination and Refinement. Diffraction data were integrated and scaled with XDS (1). The structure was solved by molecular replacement using Phaser (2). The search model was generated by pruning nonconserved residues of the neuronal Munc18-1/syntaxin 1a complex (PDB ID code 3C98; ref. 3) to alanines with Chainsaw (4). The asymmetric unit contains one Munc18/syntaxin 1 complex. The model was refined by using simulated annealing, gradient minimization, and individual isotropic B-factor refinement as implemented in Phenix (5) alternated by rebuilding cycles using the program Coot (6). In a final step, tensor elements describing the anisotropic displacement of four individual domains of Munc18 and four regions of syntaxin 1 were refined by using the Translation/Libration/Screw (TLS) implementation of Phenix. The final R factor is 0.188 with a R_{free} of 0.258. The final model comprises Munc18 residues 1–509 and 561–616, syntaxin 1 residues 2–15, 39–192, and 210–261, and 48 water molecules (Table S1). Figures were generated with the program Pymol (7). The coordinates have been deposited in the RCSB Protein Data Bank (ID code 2XHE) and will be released upon publication.

Phylogeny. Phylogenetic reconstruction was essentially done as described in ref. 8. To gain insights into the phylogenetic placement of the core factors of the secretory machinery from the choanoflagellate *M. brevicollis*, we included sequences from 15 selected animal species, 7 selected fungal species, 6 selected plant species, and 3 protists for the construction of the phylogenetic trees. The sequences of the secretory SNARE proteins (i.e., type IV) were downloaded from our SNARE database http://bioinformatics.mpibpc.mpg.de/snare. The sequences of the secretory SM proteins were gathered from the nr-database at National Center for Biotechnology Information and few genome projects from the Department of Energy Joint Genome Institute. The species list and abbreviations and the sequence identity numbers of the used sequences can be found in Table S2 and Table S3. We then aligned each factor by using muscle (9).

Phylogenetic reconstruction was composed of two different analytical approaches. The first approach used Important Quartet Puzzling and Nearest Neighbor Interchange (IQPNNI) (10) to construct phylogenetic trees from the curated alignments. We used a gamma distribution as a model for rate heterogeneity with four rate categories for the estimation of the gamma distribution parameter. The proportion of invariable sites was estimated from the data and the Jones, Taylor, and Thornton (JTT) distance matrix (11) served as a substitution matrix. We used the stopping rule of IQPNNI, but the calculation had to run for at least the suggested number of iterations. The default values were used for the remaining parameter. In addition, likelihood mapping was applied to determine the confidence of the edges in the calculated trees. The second approach used the phylip package (12) to apply a distance-based bootstrap analysis with 1,000 replicates to each of the curated alignments. Standard settings were used for seqboot, the JTT distance matrix, and also a gamma distribution (with parameter approximation from tree puzzle) for protdist, as were standard options for neighbor. If required, the random seed was set to nine. We used the almost unbiased (AU) test (13) to address the systematically biased bootstrap values. We obtained the sitewise log-likelihoods needed for the AU test by using a modified version of phyml (14), and the test was performed by using consel (15). The reconstructed IQPNNI trees served as starting points to join the results of both calculations. The inner edges of the trees were labeled with their likelihood mapping and corrected bootstrap support values.

Electrophoretic Procedures. SDS resistance of ternary SNARE complexes in polyacrylamide gels (16) was tested as described (17) with the modification that the complexes were visualized by the incorporation of synaptobrevin (1-75) labeled with the fluorescent dye Texas red at cysteine 58.

1. Kabsch W (1993) Automatic processing of rotation diffraction data from crystals of initially unknown symmetry and cell constants. *J Appl Cryst* 26:795–800.
2. McCoy AJ, Grosse-Kunstleve RW, Storoni LC, Read RJ (2005) Likelihood-enhanced fast translation functions. *Acta Crystallogr D Biol Crystallogr* 61:458–464.
3. Burkhardt P, Hattendorf DA, Weis WI, Fasshauer D (2008) Munc18a controls SNARE assembly through its interaction with the syntaxin N-peptide. *EMBO J* 27:923–933.
4. Stein N (2008) CHAINSAW: A program for mutating pdb files used as templates in molecular replacement. *J Appl Cryst* 41:641–643.
5. Adams PD, et al. (2004) Recent developments in the PHENIX software for automated crystallographic structure determination. *J Synchrotron Radiat* 11:53–55.
6. Emsley P, Cowtan K (2004) Coot: Model-building tools for molecular graphics. *Acta Crystallogr D Biol Crystallogr* 60:2126–2132.
7. DeLano WL (2002) *The PyMOL Molecular Graphics System* (DeLano Scientific, Palo Alto, CA).
8. Kloepper TH, Kienle CN, Fasshauer D (2007) An elaborate classification of SNARE proteins sheds light on the conservation of the eukaryotic endomembrane system. *Mol Biol Cell* 18:3463–3471.
9. Edgar RC (2004) MUSCLE: A multiple sequence alignment method with reduced time and space complexity. *BMC Bioinformatics* 5:113.
10. Vinh S, Von Haeseler A (2004) IQPNNI: Moving fast through tree space and stopping in time. *Mol Biol Evol* 21:1565–1571.
11. Jones DT, Taylor WR, Thornton JM (1992) The rapid generation of mutation data matrices from protein sequences. *Comput Appl Biosci* 8:275–282.
12. Felsenstein J (1998) PHYLIP - Phylogeny inference package (Version 3.2). *Cladistics* 5: 164–166.
13. Shimodaira H (2002) An approximately unbiased test of phylogenetic tree selection. *Syst Biol* 51:492–508.
14. Guindon S, Gascuel O (2003) A simple, fast, and accurate algorithm to estimate large phylogenies by maximum likelihood. *Syst Biol* 52:696–704.
15. Shimodaira H, Hasegawa M (2001) CONSEL: For assessing the confidence of phylogenetic tree selection. *Bioinformatics* 17:1246–1247.
16. Hayashi T, et al. (1994) Synaptic vesicle membrane fusion complex: Action of clostridial neurotoxins on assembly. *EMBO J* 13:5051–5061.
17. Fasshauer D, Antonin W, Margittai M, Pabst S, Jahn R (1999) Mixed and non-cognate SNARE complexes. Characterization of assembly and biophysical properties. *J Biol Chem* 274:15440–15446.
18. Dulubova I, et al. (1999) A conformational switch in syntaxin during exocytosis: Role of munc18. *EMBO J* 18:4372–4382.
19. Misura KM, Scheller RH, Weis WI (2000) Three-dimensional structure of the neuronal-Sec1-syntaxin 1a complex. *Nature* 404:355–362.
20. Munson M, Chen X, Cocina AE, Schultz SM, Hughson FM (2000) Interactions within the yeast t-SNARE Sso1p that control SNARE complex assembly. *Nat Struct Biol* 7: 894–902.
21. Margittai M, et al. (2003) Single-molecule fluorescence resonance energy transfer reveals a dynamic equilibrium between closed and open conformations of syntaxin 1. *Proc Natl Acad Sci USA* 100:15516–15521.
22. Weimer RM, et al. (2006) UNC-13 and UNC-10/rim localize synaptic vesicles to specific membrane domains. *J Neurosci* 26:8040–8047.
23. Gerber SH, et al. (2008) Conformational switch of syntaxin-1 controls synaptic vesicle fusion. *Science* 321:1507–1510.
24. Hu SH, Latham CF, Gee CL, James DE, Martin JL (2007) Structure of the Munc18c/Syntaxin4 N-peptide complex defines universal features of the N-peptide binding mode of Sec1/Munc18 proteins. *Proc Natl Acad Sci USA* 104:8773–8778.
25. Hu SH, et al. (2011) Possible roles for Munc18-1 domain 3a and Syntaxin1 N-peptide and C-terminal anchor in SNARE complex formation. *Proc Natl Acad Sci USA* 108: 1040–1045.
26. Peng RW, Guetg C, Abellan E, Fussenegger M (2010) Munc18b regulates core SNARE complex assembly and constitutive exocytosis by interacting with the N-peptide and the closed-conformation C-terminus of syntaxin 3. *Biochem J* 431:353–361.
27. Lovell SC, et al. (2003) Structure validation by Calpha geometry: Phi,psi and Cbeta deviation. *Proteins* 50:437–450.

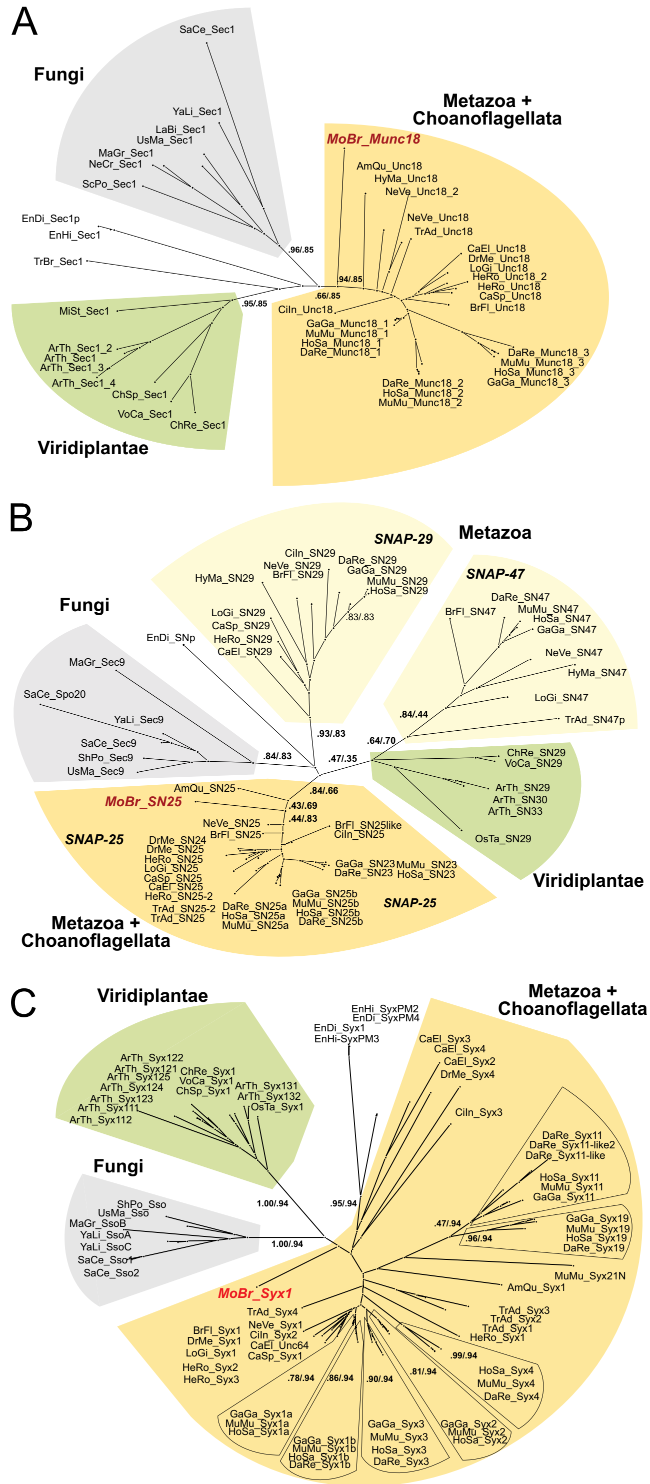

Fig. S1. Detailed versions of the phylogenetic trees of the SM protein Munc18 (*A*), the Qbc-SNARE SNAP-25 (*B*), and secretory syntaxins (*C*) (type Qa.IV) shown in Fig. 1. The major phylogenetic lineages are indicated by different colors. The labels on the major branches represent the likelihood mapping (left) and almost unbiased (AU) support values (right). The species abbreviations and sequences used are given in Table S2 and Table S3. Whereas *M. brevicollis* possesses only one factor each, duplications occurred recurrently in different animal lineages. A noteworthy expansion of Munc18-like factors occurred in vertebrates, giving rise to the three isoforms Munc18-1, -2, and -3. A more prominent expansion took place in secretory syntaxins in vertebrates (8). Interestingly, the SNAP-25–like protein found in *M. brevicollis* is closely related to the neuronal SNAP-25 of animals (8), whereas the sequences of the other two Qbc-SNAREs animal homologs SNAP-29 and SNAP-47, have diverged substantially.

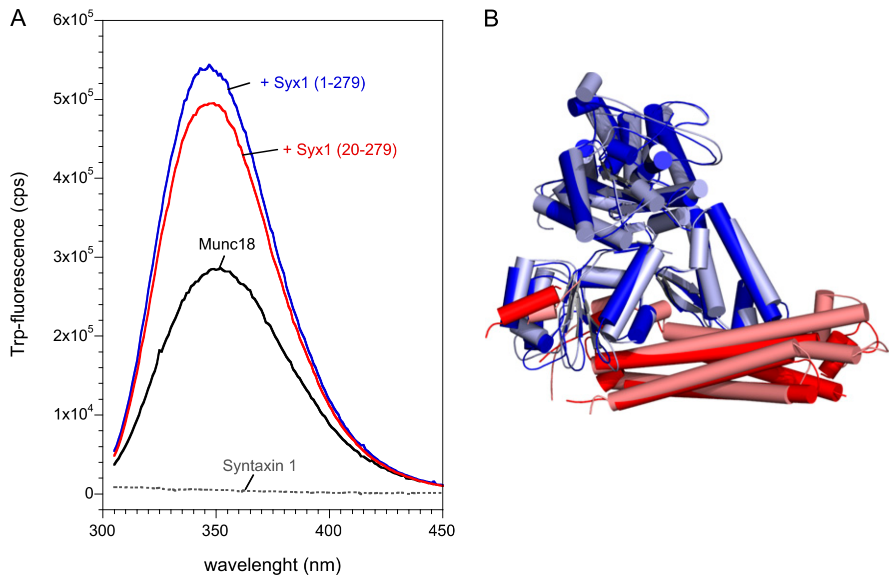

Fig. S2. Change of intrinsic fluorescence upon binding of Munc18 to syntaxin 1 (*A*) and overlay of the Munc18/Syx1 complexes (*B*). (*A*) Baseline corrected tryptophan fluorescence emission spectra of Syx1 (1-279), Munc18, Munc18 mixed with Syx1 (1-279), and Munc18 mixed with Syx1 (20-279) (500 nM each) after excitation at 295 nm. Upon addition of Syx1 (1-279) or Syx1 (20-279) to Munc18-1, an increase in fluorescence was monitored. Note that syntaxin 1 does not posses a tryptophan. Interestingly, the increase in tryptophan fluorescence in the presence of Syx1 (20-279) was somewhat less pronounced than in the presence of Syx1 (1-279). A similar difference in the fluorescence change was observed for the rat homologs. This change in fluorescence suggests that both syntaxin variants adopt a slightly different conformation in complex with Munc18. It seems likely that the increase in tryptophan fluorescence is caused by close proximity of Trp-24 of *M. brevicollis* Munc18 (Trp-28 of rat Munc18-1) and Phe-46 and Phe-47 of *M. brevicollis* syntaxin 1 (Phe-33 and Phe-34 of rat Syx1a). (*B*) Overlay of the Munc18/Syx1 complexes from *M. brevicollis* (Munc18, blue; Syx1, red) and from *R. norvegicus* (Munc18-1, light blue; Syx1a, salmon; PDB ID code 3C98) reveals their overall similarity.

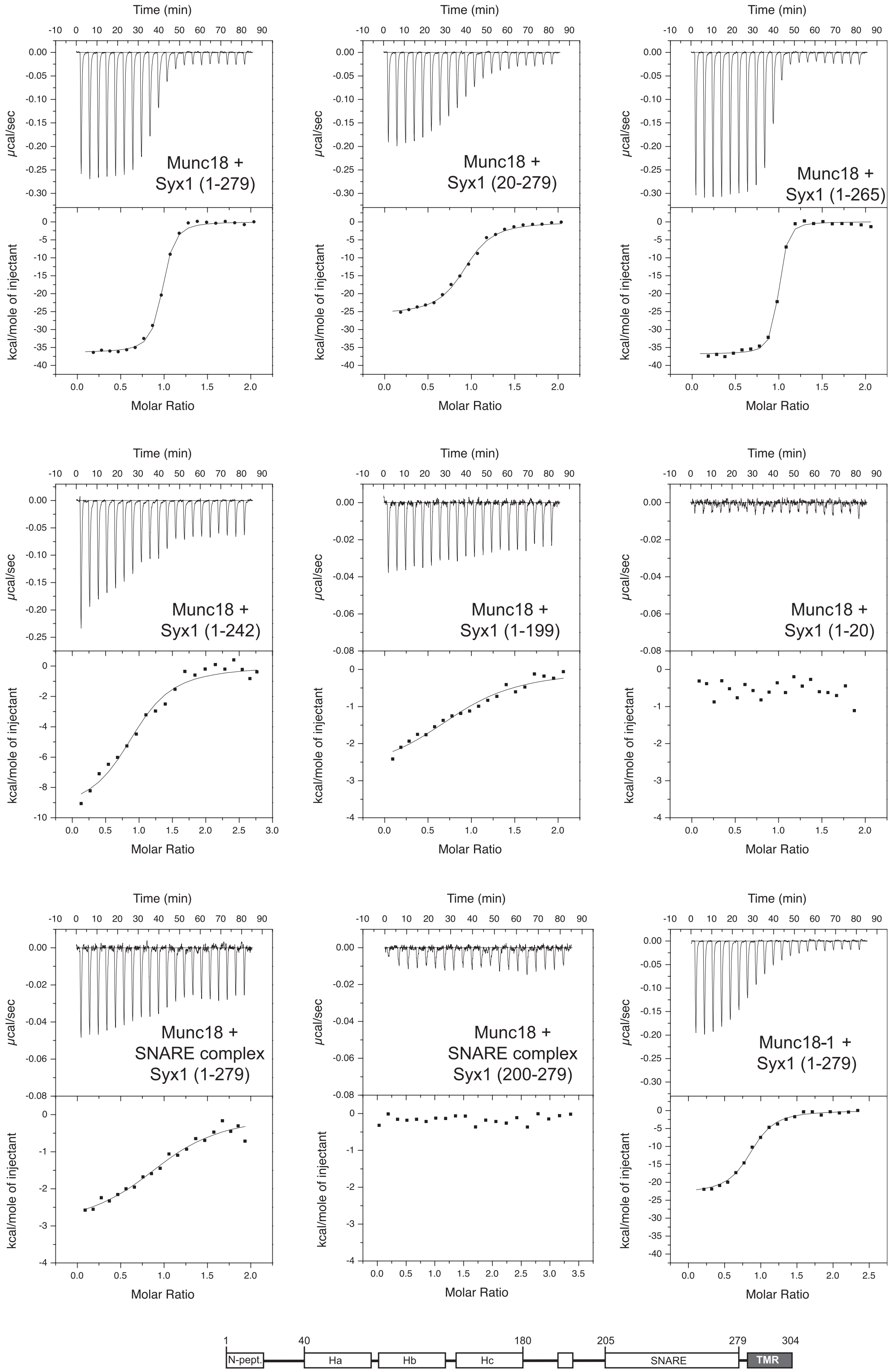

Fig. S3. Isothermal titration calorimetry data for the interaction of syntaxin 1 and Munc18. All isothermal calorimetric experiments were performed at 25 °C in PBS buffer. In each titration, the syntaxin 1 variant or syntaxin 1 assembled into a purified ternary SNARE complex was injected into Munc18 from *M. brevicollis* or Munc18-1 from *Rattus norvegicus* (*Bottom*). In each graph, *Upper* shows the base-line corrected raw data in power versus time during the injections. *Lower* displays the integrated areas normalized to the amount of the injectant (kcal·mol^{-1}) versus its molar ratio to Munc18. The solid lines represent the best fit to the data for a single binding site model by using a nonlinear least squares fit. The results of the fits are given in Table 1. For experiments performed in replicate, a representative example is shown. Most titrations using individual syntaxin 1 variants were carried out at 20 µM syntaxin 1 and 2.5 µM Munc18. A higher concentration was used (50 µM and 4 µM, respectively) for Syx1 (1-242) and (40 µM and 4 µM, respectively) for Syx1 (1-199) to account for the smaller heat changes upon interaction with Munc18. Similarly, 30 µM and 3.5 µM, respectively, were used for titrating purified SNARE complexes and Munc18.

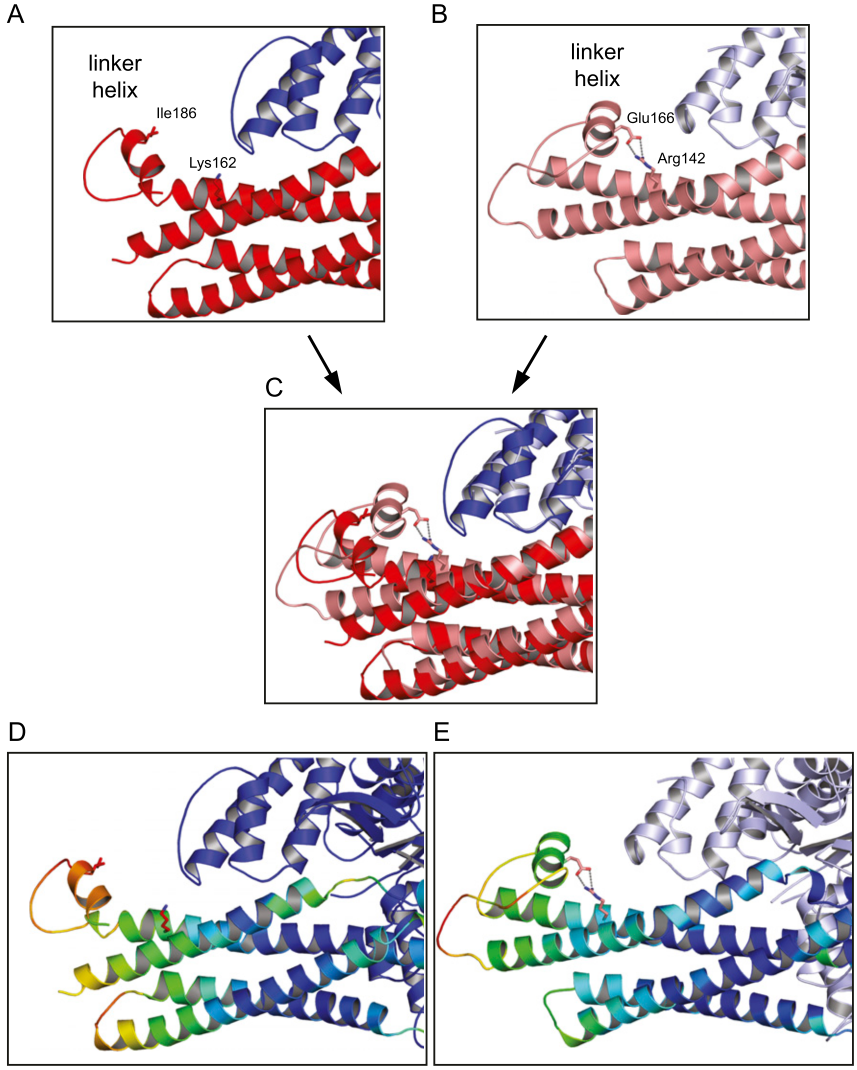

Fig. S4. Different conformations of the linker helix in the Munc18/syntaxin 1 complexes from *Monosiga brevicollis* and *Rattus norvegicus*. Different conformation of the linker helix of syntaxin1 from *M. brevicollis* (*A*) and from *R. norvegicus* (PDB ID code 3C98; ref. 3) (*B*). An overlay of the two structures is shown in *C*. In the structure from *R. norvegicus,* the orientation of the linker helix of syntaxin 1a is stabilized by the residues Glu166 of the linker helix and Arg142 of the Hb helix. This interaction is thought to stabilize the closed conformation of syntaxin 1a (18, 19). In the *M. brevicollis* structure, the corresponding residues, Ile186 and Lys162, do not interact. Nevertheless, syntaxin 1 from *M. brevicollis* adopts a closed conformation in the Munc18/syntaxin 1 complex. Interestingly, the linker of *M. brevicollis* syntaxin appears to be slightly more flexible compared with the one of rat. In fact, we observed that residues of the linker helix exhibit elevated temperature factors compared with the rest of the model (*D*), whereas the residues of the linker helix of the structure from *R. norvegicus* do not display elevated temperature factors (*E*). This difference possibly explains why the block of SNARE assembly exerted by Munc18 from *M. brevicollis* is somewhat less efficient than observed for the vertebrate homologs. Incidentally, the yeast syntaxin Sso1 has been found in a tight closed conformation in the absence of its SM partner Sec1 (20). Sso1's closed conformation is stabilized by multiple intermolecular contacts, whereas the closed conformation of syntaxin 1 of *R. norvegicus* and of *M. brevicollis* appears to be reinforced by Munc18. In fact, in isolation, rat syntaxin 1 rapidly switches between an open and closed conformation, with the majority of molecules being open (21). Of note, a double mutation in the aforementioned linker region, L165A/E166A (Syx1a^{LE}) was used in several studies. Because this mutation was originally proposed to open up syntaxin 1a (18), it was anticipated that it would not require the activity of Munc18. Unexpectedly, however, Syx1^{LE} turned out to be unable to bypass the requirement for Unc18 in *C. elegans* (22). Remarkably, Munc18a-1 nonetheless tightly enfolds Syx1a^{LE} (3), presumably in a closed conformation, yet is unable to stop it from forming a SNARE complex. It seems possible that Syx1a^{LE} in complex with Munc18 adopts a less rigid closed conformation, which permits SNARE complex assembly independent of whether its *N*-peptide is bound to the outer surface of Munc18-1 (3). The less rigid closed conformation is supported by the somewhat smaller intrinsic fluorescence change observed for the mutant upon binding to Munc18-1 (3). In this context. it is interesting to note that knockout/knockin mice that express only Syx1b^{LE} showed an enhanced fusogenicity of synaptic vesicles (23), supporting the view that Munc18-1 lost some of its control over the accessibility of syntaxin.

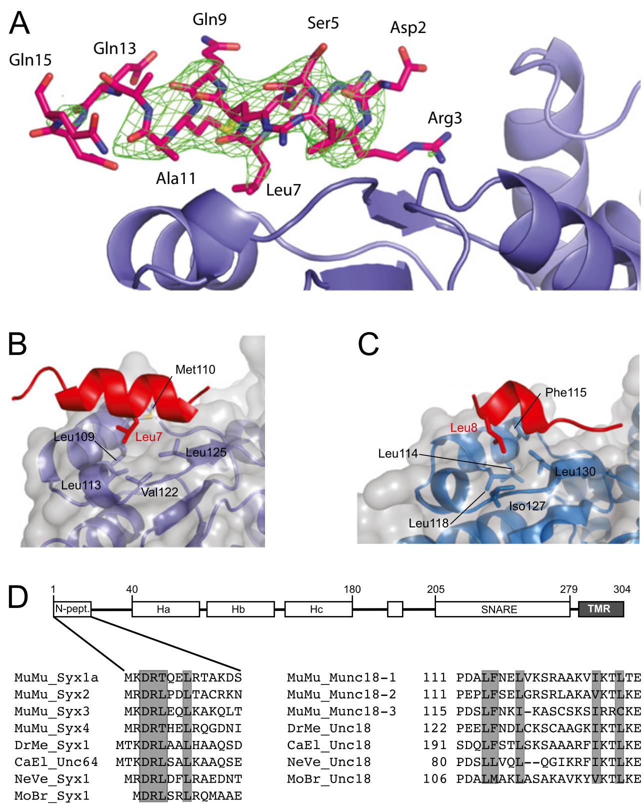

Fig. S5. The syntaxin 1 *N*-peptide binds to the outer surface of Munc18. (*A*) F_{obs}-F_{calc} omit map of the *M. brevicollis* Syx1 *N*-peptide region contoured at 3σ (green mesh). The final model is shown as sticks (carbon: pink). Blue: *M. brevicollis* Munc18 displayed as cartoon. (*B* and *C*) Detailed view on the *N*-peptide binding pocket of the choanoflagellate and the vertebrate Munc18/syntaxin 1 complex. In *M. brevicollis*, Leu7 packs into a hydrophobic pocket formed by the residues Leu109, Met110, Leu113, Val122, and Leu125 of Munc18. The *N*-peptide is shown in red and domain 1 of Munc18 in blue (*B*). In *R. norvegicus*, the corresponding residue Leu8 sandwiches into the homologous hydrophobic pocket formed by the residues Leu114, Phe115, Leu118, Ile127, and Leu130. Interestingly, the ordered region of the bound *N*-peptide of syntaxin 1 is slightly longer in *M. brevicollis* (comprising residues 2–15) as in the Munc18-1-syntaxin 1a structure (residues 2–9). The overall structure of the bound syntaxin 1 *N*-peptide is similar to that of syntaxin 4 bound to Munc18-3 (24, 25), but note that so far no structure of Munc18-3 with the remainder of syntaxin 4 is available. When comparing the structure and working of the orthologous Munc18/syntaxin pairs of vertebrates, it should also be kept in mind that all three Munc18 orthologs in vertebrates originate from a single gene. Likewise, the different secretory syntaxins of vertebrates arose from gene duplications during the rise of vertebrates, suggesting that they function similarly (see, for example, ref. 26). (*D*) Schematic drawing of the domain structure of *M. brevicollis* syntaxin 1. Sequence alignments of the *N*-peptide of syntaxin (*Left*) and of the conserved *N*-peptide binding site in Munc18 (*Right*) from mice, fly, nematode, sea anemone, and choanoflagellate are shown. Note that the *N*-peptide of syntaxin 1 from *M. brevicollis* possesses a highly conserved DRL/TxxL-motif.

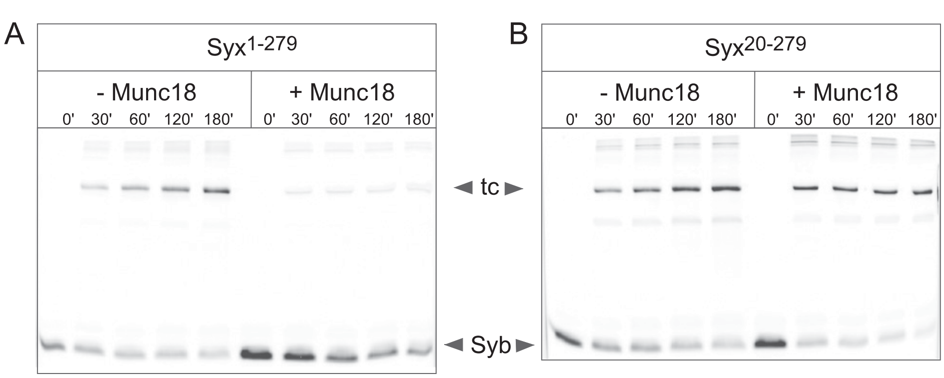

Fig. S6. Assembly of SDS-resistant SNARE complexes for syntaxin with (Syx1-279) and without *N*-peptide (Syx20-279) in the absence or presence of Munc18. Assembly of SNARE complexes in the absence or presence of Munc18 was monitored by the formation of SDS-resistant complexes (tc) containing synaptobrevin labeled with the fluorescent dye Texas red at Cys58. For both syntaxin 1 variants, Syx1 (1-279) and Syx1 (20-279), SNARE complexes formed in the absence of Munc18. In the presence of Munc18, however, SNARE complex formation was inhibited for Syx1 (1-279) (*A*), whereas a clear SDS-resistant band was visible for Syx1 (20-279) (*B*).

Table S1. Crystallographic data and refinement statistics

Measurement	Value
Wavelength, Å	1.0385
Temperature, K	100
Space group	$P6_522$
Unit cell parameters, Å	
a, *b*	146.2
c	214.8
Resolution, Å	35.0–2.8 (2.9–2.8)
Reflections	
Unique	30,089
Completeness, %	99.9 (100)
Redundancy	14.7 (14.3)
Mean $I/\sigma(I)$	19.8 (2.1)
$R_{sym}(I)$*, %	10.0 (75.4)
Refinement	
Resolution, Å	35.0–2.8
Reflections	
Number	30,041
Completeness, %	99.9
Test set, %	5
R_{work}†, %	18.8
R_{free}†, %	25.0
ESU, Å	0.39
Contents of A.U.	
Complexes/protein molecules/residues/ atoms	1/2/835/6,315
Water oxygens	48
Mean B factors, $Å^2$	
Wilson	75.2
Protein	104.8
Water	70.8
Ramachandran plot‡, %	
Preferred	89.3
Allowed	8.7
Disallowed	2.0
rmsd from target geometry	
Bond lengths, Å	0.007
Bond angles, °	1.069
Chirality, Å	0.075
Dihedral angles, °	18.07
PDB ID code	2XHE

Data for the highest resolution shell in parentheses. ESU, estimated overall coordinate error based on maximum likelihood; A.U., asymmetric unit; rmsd, root-mean-square deviation.

*$R_{sym}(I) = \Sigma_{hkl}\Sigma_i|I_i(hkl) - \langle I(hkl)\rangle| / \Sigma_{hkl}\Sigma_i|I_i(hkl)|$; for *n* independent reflections and *i* observations of a given reflection; $\langle I(hkl)\rangle$ – average intensity of the *i* observations.

†$R = \Sigma_{hkl}||F_{obs}| - |F_{calc}|| / \Sigma_{hkl}|F_{obs}|$; R_{work}, hkl $\notin$ T; R_{free}, hkl $\in$ T; R_{all}, all reflections; T, test set.

‡According to ref. 27.

Table S2. Species list and abbreviations

Species	Abbreviation
Amphimedon queenslandica	AmQu
Arabidopsis thaliana	ArTh
Branchiostoma floridae	BrFl
Caenorhabditis elegans	CaEl
Capitella sp. 1	CaSp
Chlamydomonas reinhardtii	ChRe
Chlorella sp. NC64A	ChSp
Ciona intestinalis	CiIn
Danio rerio	DaRe
Drosophila melanogaster	DrMe
Entamoeba dispar SAW760	EnDi
Entamoeba histolytica HM-1:IMSS	EnHi
Gallus gallus	GaGa
Hellobdella robusta	HeRo
Homo sapiens	HoSa
Hydra magnipapillata	HyMa
Laccaria bicolor S238N-H82	LaBi
Lottia gigantea	LoBi
Magnaporthe grisea 70–15	MaGr
Micromonas sp. RCC299	MiSt
Monosiga brevicollis	MoBr
Mus musculus	MuMu
Nematostella vectensis	NeVe
Neurospora crassa N150	NeCr
Ostreococcus tauri	OsTa
Saccharomyces cerevisiae	SaCe
Schizosaccharomyces pombe	ScPo
Trichoplax adhaerens	TrAd
Trypanosoma brucei TREU927	TrBr
Ustilago maydis 521	UsMa
Volvox carteri f. nagariensis	VoCa
Yarrowia lipolytica CLIB99	YaLi

Table S3. Identity of used sequences

Name	Species	Database source	Identification no.
Secretory SM proteins			
HoSa_Munc18_1a	*Homo sapiens*	NCBI_nr	4507297
CaEl_Unc18	*Caenorhabditis elegans*	NCBI_nr	71988800
GaGa_Munc18_1	*Gallus gallus*	NCBI_nr	46195820
MuMu_Munc18_2	*Mus musculus*	NCBI_nr	6755688
TrBr_Sec1	*Trypanosoma brucei* TREU927	NCBI_nr	71744018
MiSt_Sec1	*Micromonas* sp. RCC299	NCBI_nr	255089845
HeRo_Unc18_2	*Hellobdella robusta*	DOE JGI	Helro1|187018
LoGi_Unc18	*Lottia gigantea*	DOE JGI	Lotgi1|237771
EnDi_Sec1_part	*Entamoeba dispar* SAW760	NCBI_nr	167384806
DaRe_Munc18_2	*Danio rerio*	NCBI_nr	47086919
VoCa_Sec1	*Volvox carteri* f. nagariensis	DOE JGI	Volca1|67807
GaGa_Munc18_3	*Gallus gallus*	NCBI_nr	119331098
BrFl_Unc18	*Branchiostoma floridae*	NCBI_nr	219459049
AmQu_Unc18	*Amphimedon queenslandica*	Compagen, Assembled by hand	
NeVe_Unc18	*Nematostella vectensis*	NCBI_nr	156390747
NeCr_Sec1	*Neurospora crassa* N150	NCBI_nr	85108189
ArTh_Sec1	*Arabidopsis* thaliana	NCBI_nr	18391384
HyMa_Unc18	*Hydra magnipapillata*	NCBI_nr	221121424
SaCe_Sec1	*Saccharomyces cerevisiae*	NCBI_nr	6320368
MaGr_Sec1	*Magnaporthe grisea* 70–15	NCBI_nr	145612411
LaBi_Sec1	*Laccaria bicolor* S238N-H82	NCBI_nr	170087878
DrMe_Unc18	*Drosophila melanogaster*	NCBI_nr	24657265
ArTh_Sec1_4	*Arabidopsis thaliana*	NCBI_nr	7267913
EnHi_Sec1	*Entamoeba histolytica* HM-1:IMSS	NCBI_nr	56464018
MuMu_Munc18_1a	*Mus musculus*	NCBI_nr	165972307
TrAd_Unc18	*Trichoplax adhaerens*	NCBI_nr	196000262
ChSp_Sec1	*Chlorella* sp. NC64A	DOE JGI	ChlNC64A_1|56812
ScPo_Sec1	*Schizosaccharomyces pombe*	NCBI_nr	19075726
DaRe_Munc18_3	*Danio rerio*	NCBI_nr	47087331
UsMa_Sec1	*Ustilago maydis* 521	NCBI_nr	71019769
ChRe_Sec1	*Chlamydomonas reinhardtii*	NCBI_nr	158273495
DaRe_Munc18_1	*Danio rerio*	NCBI_nr	68448507
MoBr_Munc18	*Monosiga brevicollis* MX1	NCBI_nr	167523609
HoSa_Munc18_3	*Homo sapiens*	NCBI_nr	118600975
MuMu_Munc18_3a	*Mus musculus*	NCBI_nr	6755690
CiIn_Unc18	*Ciona intestinalis*	NCBI_nr	198429537
HoSa_Munc18_2a	*Homo sapiens*	NCBI_nr	188528689
NeVe_Unc18_2	*Nematostella vectensis*	NCBI_nr	156390749
ArTh_Sec1_3	*Arabidopsis thaliana*	NCBI_nr	18413751
ArTh_Sec1_2	*Arabidopsis thaliana*	NCBI_nr	145334974
CaSp_Unc18_1	*Capitella* sp. 1	DOE JGI	Capca1|150412
YaLi_Sec1	*Yarrowia lipolytica* CLIB99	NCBI_nr	50553686
HeRo_Unc18	*Hellobdella robusta*	DOE JGI	Helro1|66166
Qbc-SNARE			
MuMu_SN29	*Mus musculus*	NCBI_nr	31543752
LoGi_SN25	*Lottia gigantea*	DOE JGI	Lotgi1|197810
HeRo_SN25-2	*Hellobdella robusta*	DOE JGI	Helro1|71107
GaGa_SN23	*Gallus gallus*	NCBI_nr	50748211
HeRo_SN29	*Hellobdella robusta*	DOE JGI	Helro1|184904
UsMa_Sec9	*Ustilago maydis* 521	NCBI_nr	49072430
CaEl_SN25	*Caenorhabditis elegans*	NCBI_nr	32567202
HyMa_SN29	*Hydra magnipapillata*	NCBI_est	46968126
ArTh_SN33	*Arabidopsis thaliana*	NCBI_nr	15240163
GaGa_SN47	*Gallus gallus*	NCBI_nr	50732155
HoSa_SN29	*Homo sapiens*	NCBI_nr	4759154
DrMe_SN25	*Drosophila melanogaster*	NCBI_nr	1763657
BrFl_SN47	*Branchiostoma floridae*	DOE JGI	Brafl1|240128
MuMu_SN47	*Mus musculus*	NCBI_nr	21362303
MuMu_SN23	*Mus musculus*	NCBI_nr	6678049
TrAd_SN25-2	*Trichoplax adhaerens*	DOE JGI	Triad1|63490
HyMa_SNx	*Hydra magnipapillata*	NCBI_est	47136750
CaEl_SN29	*Caenorhabditis elegans*	NCBI_nr	17554000

Table S3. Cont.

Name	Species	Database source	Identification no.
NeVe_SN29	*Nematostella vectensis*	DOE JGI	Nemve1|108962
GaGa_SN25b	*Gallus gallus*	NCBI_nr	45382033
CaSp_SN25	*Capitella* sp. 1	DOE JGI	Capca1|180292
HoSa_SN25a	*Homo sapiens*	NCBI_nr	18765733
ArTh_SN30	*Arabidopsis thaliana*	NCBI_nr	15222976
HeRo_SN25	*Hellobdella robusta*	DOE JGI	Helro1|155336
LoGi_SN29	*Lottia gigantea*	DOE JGI	Lotgi1|237114
LoGi_SN47	*Lottia gigantea*	DOE JGI	Lotgi1|172501
BrFl_SN29	*Branchiostoma floridae*	NCBI_est	66378306
TrAd_SN47p	*Trichoplax adhaerens*	DOE JGI	Triad1|55100
CaSp_SN29	*Capitella* sp. 1	DOE JGI	Capca1|19521
DrMe_SN24	*Drosophila melanogaster*	NCBI_nr	17737875
AmQu_SN25	*Amphimedon queenslandica*	Compagen, Assembled by hand	
NeVe_SN47	*Nematostella vectensis*	NCBI, Assembled by hand	
TrAd_SN25	*Trichoplax adhaerens*	DOE JGI	Triad1|51809
CiIn_SN25	*Ciona intestinalis*	DOE JGI	Cioin2|294632
BrFl_SN25	*Branchiostoma floridae*	NCBI_est	66384552
BrFl_SN25like	*Branchiostoma floridae*	DOE JGI	Brafl1|84606
CiIn_SN29	*Ciona intestinalis*	DOE JGI	Cioin2|275649
HoSa_SN47	*Homo sapiens*	NCBI_nr	37589927
SaCe_Sec9	*Saccharomyces cerevisiae*	NCBI_nr	6321446
EnDi_SNp	*Entamoeba dispar* SAW760	NCBI_nr	167395986
DaRe_SN23	*Danio rerio*	NCBI_nr	41055690
MoBr_SN25	*Monosiga brevicollis*	DOE JGI	JGI_XYM16904.rev
HoSa_SN25b	*Homo sapiens*	NCBI_nr	18765735
ShPo_Sec9	*Schizosaccharomyces pombe*	NCBI_nr	19113435
DaRe_SN29	*Danio rerio*	NCBI_nr	63102202
DaRe_SN25a	*Danio rerio*	NCBI_nr	37589801
NeVe_SN25	*Nematostella vectensis*	DOE JGI	Nemve1|229104
HoSa_SN23	*Homo sapiens*	NCBI_nr	18765729
ChRe_SN29	*Chlamydomonas reinhardtii*	DOE JGI	Chlre3|155582
GaGa_SN29	*Gallus gallus*	NCBI_nr	50756211
MuMu_SN25a	*Homo sapiens*	NCBI_nr	54696236
EnDi_SnpOrNpsn	*Entamoeba dispar* SAW760	NCBI_nr	165893407
MuMu_SN25b	*Mus musculus*	NCBI_nr	6755588
DaRe_SN25b	*Danio rerio*	NCBI_nr	70887763
VoCa_SN29	*Volvox carteri* f. nagariensis	DOE JGI	Volca1|104786
SaCe_Spo20	*Saccharomyces cerevisiae*	NCBI_nr	6323659
ArTh_SN29	*Arabidopsis thaliana*	NCBI_nr	15241436
DaRe_SN47	*Danio rerio*	NCBI_nr	68404785
OsTa_SN25	*Ostreococcus tauri*	DOE JGI	Ostta4|36669
MaGr_Sec9	*Magnaporthe grisea* 70–15	NCBI_nr	38101969
YaLi_Sec9	*Yarrowia lipolytica* CLIB99	NCBI_nr	50553382